Colloquium: Condensed phases of gases inside nanotube bundles

M. Mercedes Calbi and Milton W. Cole

Department of Physics, Pennsylvania State University, University Park, Pennsylvania 16802

Silvina M. Gatica

Departmento de Física, Facultad de Ciencias Exactas y Naturales, Universidad de Buenos Aires, 1428 Buenos Aires, Argentina

Mary J. Bojan

Department of Chemistry, Pennsylvania State University, University Park, Pennsylvania 16802

George Stan

Institute for Physical Science and Technology, and Department of Chemical Engineering, University of Maryland, College Park, Maryland 20742

(Published 15 November 2001)

An overview is presented of the various phases predicted to occur when gases are absorbed within a bundle of carbon nanotubes. The behavior may be characterized by an effective dimensionality, which depends on the species and the temperature. Small molecules are strongly attracted to the interstitial channels between tubes. There, they undergo transitions between ordered and disordered quasi-one-dimensional (1D) phases. Both small and large molecules display 1D and/or 2D phase behavior when adsorbed within the nanotubes, depending on the species and thermodynamic conditions. Finally, molecules adsorbed on the external surface of the bundle exhibit 1D behavior (striped phases), which crosses over to 2D behavior (monolayer film) and eventually 3D behavior (thick film) as the coverage is increased. The various phases exhibit a wide variety of thermal and other properties.

CONTENTS

I. INTRODUCTION

A carbon nanotube is a cylindrical tube, of typical radius between 5 and 10 Å, consisting of one or more concentric rolled up planes of graphite. The discovery of such tubes by Iijima, in 1991, has elicited numerous ideas of interest to both fundamental and applied scientists (Dresselhaus *et al.*, 1996). For physicists, much of the excitement has focused on the possibility of observing novel one-dimensional (1D) behavior, a consequence of the remarkable aspect ratio ($\approx 10^4$) of the length of the tubes to their radius. Such 1D behavior is expected for both the tubes themselves and any gas imbibed within the tubes; the latter is the subject of this Colloquium. Specifically, we explore the phases of the adsorbate present at each of the various sites of a bundle (or "rope") of carbon nanotubes depicted in Fig. 1. These three regions, assumed to contribute additively to the gas uptake, are inside a tube, within an interstitial channel (the space between tubes, abbreviated IC) and the external surface of the bundle. We shall see in this Colloquium that various phases have been predicted whose properties are quite remarkable. Experimental tests of these predictions are under way in many laboratories (Dresselhaus *et al.*, 1999; Teizer *et al.*, 1999, 2000; Bienfait *et al.*, 2000; Kuznetsova *et al.*, 2000; Muris *et al.*, 2000; Talapatra *et al.*, 2000; Weber *et al.*, 2000). Here, we focus on qualitative aspects of the predictions without providing a detailed explanation of the theoretical methods used to derive them. The key assumptions used in the calculations (e.g., that the nanotube lattice is perfectly ordered) are discussed in the final section of this Colloquium.

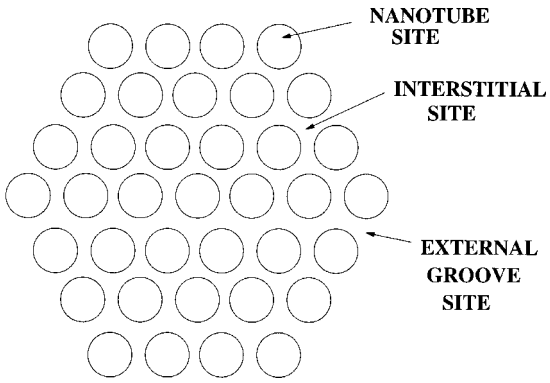

FIG. 1. Schematic depiction of a bundle of 37 nanotubes, of radius 7 Å. This bundle contains 54 interstitial channels and 18 "grooves" on the external surface.

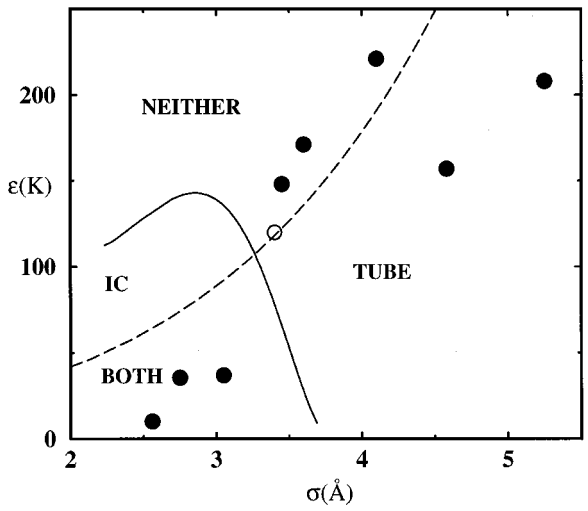

FIG. 2. Location (within interstitial channel and/or tube) of absorbed atoms or molecules within a bundle of tubes of radius 8 Å, as a function of the Lennard-Jones parameters which characterize the interactions between adsorbates. Dots correspond to a sequence of increasing values of σ as follows: He, Ne, H_2, Ar (open circle), CH_4, Kr, Xe, CF_4, and SF_6. Molecular species with strongly cohesive interactions (large ϵ, i.e., CH_4, Kr, Xe) do not absorb at either site at the assumed thermodynamic conditions: reduced temperature $T^*=1$ and reduced chemical potential (relative to saturation) $\Delta\mu^*=(\mu-\mu_0)/\epsilon=-10$ (Stan *et al.*, 2000).

The word "dimension" should be used with some caution in describing these phenomena. In statistical mechanics, a system is usually characterized as "D dimensional" if D equals the number of spatial dimensions which diverge when the thermodynamic limit is taken. In the following, the geometry is fixed as that shown in Fig. 1, a hexagonal array of nanotubes. The length of the tubes is assumed to be infinite. We shall see how temperature (T) influences the observed dimensionality of the adsorbate. This happens, for example, when certain degrees of freedom are effectively frozen out at low T, leaving only excitations characterized by a reduced dimensionality. This change of effective dimension D affects the power-law behavior and the critical exponents characterizing the divergent behavior of thermodynamic properties at phase transitions. The value of D may either increase or decrease as a function of T. In two cases discussed below (single particle and phonon excitations), D is an increasing function of T, while in another (condensation transition) it is a decreasing function of T.

A typical adsorption experiment involves the presence of a known vapor that is brought into contact with the nanotube bundle. An obvious question arises: at a given T and external pressure (P), how much gas goes into each of the various sites? Figure 2 presents the results of model calculations of the uptake of various gases, assuming equilibrium between the absorbed and the external gases. Each species of gas has an interatomic interaction $V(r)$ characterized by energy (ϵ) and length (σ) parameters. Typically, but not always, one assumes that this has the Lennard-Jones form:

$$V(r)=4\epsilon\{[\sigma/r]^{12}-[\sigma/r]^6\}. \tag{1}$$

It is usual to assume that the interaction between the gas and the carbon atoms of the nanotube satisfy combining rules of the form $\sigma_{gC}=(\sigma+\sigma_C)/2$ and $\epsilon_{gC}=\sqrt{\epsilon\epsilon_C}$ with $\sigma_C\approx 3.4$ Å and $\epsilon_C\approx 28$ K. With these interactions, one can compute the gas uptake within the nanotubes and interstitial channels.

One observes in Fig. 2 that species having small values of σ (i.e., He, Ne, and H_2) absorb significantly within the interstitial channels while larger molecules do not. The word "significant" is defined here to mean that the average spacing (inverse 1D density) between molecules is less than 10 σ. The σ-dependent behavior seen in Fig. 2 is a logical consequence of a key assumption used to create the figure: that the bundle of tubes does not deform (e.g., swell) during the absorption process. Hence, large molecules do not fit within the interstitial channels.

Both these small and quite large (CF_4 and SF_6) molecular species are seen in Fig. 2 to absorb strongly inside the tubes. In contrast, intermediate size gases (CH_4, Kr, and Xe) do not populate the tubes significantly at the assumed pressure and temperature ($T^*=k_BT/\epsilon=1$), although they do at somewhat lower temperature and higher pressure. The determinant of this systematic behavior is a competition between adhesive forces, favoring uptake, and cohesive forces, which oppose uptake; these latter predominate at large values of ϵ, as seen in the figure. Ar (shown as an open circle in Fig. 2) is a system for which these competing factors are comparable; its 1D density at the conditions of Fig. 2 is $0.1/\sigma$, so it is a borderline case.

The adsorbate's behavior within each region of space is a function of the number of molecules there. What we know for certain is that the total number N of absorbed molecules increases with pressure P. An important thermodynamic parameter characterizing this dependence is the chemical potential

$$\mu=\left(\frac{\partial F}{\partial N}\right)_T, \tag{2}$$

where F is the Helmholtz free energy. In equilibrium, the chemical potentials of the coexisting adsorbate and vapor phases coincide. For an ideal gas at temperature T, we have the relation

$$\beta\mu=\ln(\beta P\lambda^3), \tag{3}$$

where $\beta\equiv 1/(k_BT)$ and λ is the de Broglie thermal wavelength, i.e., a typical particle's wavelength:

$$\lambda^2=\frac{2\pi\beta\hbar^2}{m}, \tag{4}$$

m being the mass of the particle.[1] A benchmark for the chemical potential is its value (μ_0) at saturated vapor pressure. Capillary condensation is the formation of liquid within pores at $\mu<\mu_0$.

[1]Equation (3) assumes that the gas is monatomic and spinless. Otherwise, the argument of the logarithm is to be divided by the internal partition function of the adsorbate.

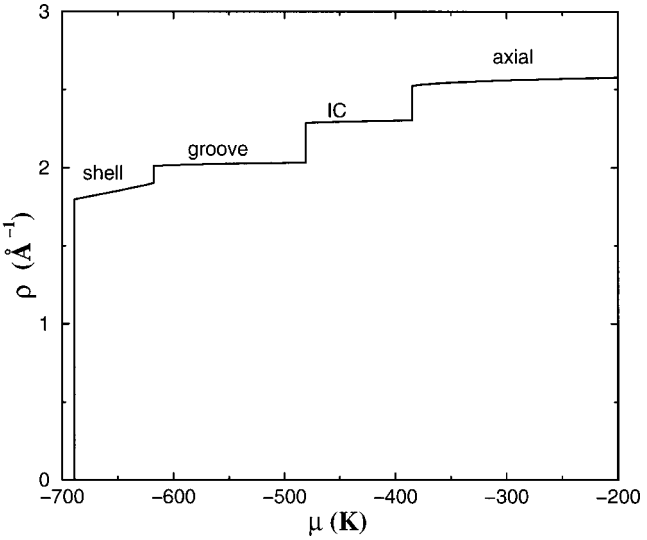

FIG. 3. H_2 absorption (per unit length of nanotube) as a function of chemical potential μ. The indicated plateau regions correspond to the progressive filling of various distinct domains within the nanotube bundle (shown in Fig. 1). At the highest chemical potential shown, the mass of H_2 is 2.6% of the total mass of the system (tubes plus gas). A linear H_2 density $\rho=1$ Å^{-1} corresponds to 5 mmoles of H_2 per gram of carbon. Derived from data of Stan *et al.* (2000) and Calbi *et al.* (2000).

The task of the theory is to compute how μ of the adsorbate varies with N; using Eq. (3), one can then predict the dependence of N on P. Conversely, experiments (adsorption isotherms) which measure $N(P)$ yield the chemical potential of the adsorbate. This is an important goal because all thermodynamic variables characterizing the film can be derived from $\mu(N,T)$, since its integral over N is the free energy F, from which other thermodynamic properties can be computed. More interesting, perhaps, is that the structure of the film can often be deduced by judicious interpretation of the μ data. Figure 3 exemplifies this; the $T=0$ isotherm for H_2 is seen to exhibit a series of steps, due to a succession of absorption phenomena: covering the nanotube interior walls ("shell" phase), filling the groove on the outside of the bundle, filling the interstitial channels, filling the axial region of the tubes, and eventually fully covering the outside of the bundle at higher chemical potential than is shown in the figure. The size of each step is equal to the number of molecules "filling" each site. This site capacity, per unit length of bundle, is equal to a product of the 1D density within the site and the number of equivalent sites within the bundle. If we let j equal the number of tubes on each facet bounding the bundle, assumed to be hexagonal ($j=4$ in Fig. 1), then one may prove that the number of external grooves is $6(j-1)$, the number of interstitial channels is $6[j(j-2)+1]$ and the number of tubes is $1+3j(j-1)$. For large j, there are twice as many interstitial chanels as tubes. We note that the steps seen in Fig. 3 become progressively rounded as T increases.

One of the practical motivations for studying adsorption in nanotubes is their potential for high storage capacity of various gases. While not the focus of this Colloquium it is worthwhile to discuss this topic briefly. There are several encouraging aspects to this pursuit. One is that graphitic materials provide a particularly strong attraction as compared with other adsorbents (Bruch *et al.*, 1997). A second is that curved surfaces provide relatively attractive binding environments compared to planar surfaces. Finally, and most significantly, single wall carbon nanotubes are optimally efficient adsorbents on a "per gram" basis. The reason is quite simple: they are "all surface" (Williams and Eklund, 2000; Dillon and Heben, 2001). For example, in Fig. 3, the uptake at quite low chemical potential (far below saturation) exceeds 10 mmole/gr. A typical "high surface area" material, such as grafoil, adsorbs ≈ 0.5 mmole/gr under these conditions. Thus the nanotubes provide an order of magnitude increase in storage capacity.

In the following sections, we describe results of calculations of phase behavior and other properties within the various regions of space where the particles are absorbed. We ignore almost entirely the methodology of the calculations; the interested reader may turn to the original sources. We focus on predictions of the phase behavior since experiments have only begun to test these predictions. One of the principal obstacles to such tests is the difficulty of making high quality, low impurity samples. Fortunately, there has been significant progress recently in this regard (Schlittler *et al.*, 2001).

II. GASES WITHIN INTERSTITIAL CHANNELS

As indicated in Fig. 2, we anticipate that He, Ne, and H_2 will adsorb within the interstitial channels in large numbers. What properties do we expect to observe? The molecules are confined to the vicinity of the z axis, defined to lie at the center of a given interstitial channel, and thus 1D behavior is predicted (Stan *et al.*, 1998). Figure 4 depicts the potential energy experienced by an H_2 molecule as it moves away from the axis and the corresponding wave function, which extends only ≈ 0.2 Å from this axis.[2]

Such a high degree of confinement suggests a 1D interpretation of the behavior. Interestingly, two extreme alternative 1D models have been employed to characterize this system. A "quasifree" model neglects any z dependence of the potential energy. A "localized" model [which has been justified by a band-structure calculation for one specific array of tubes (Cole *et al.*, 2000; Boninsegni *et al.*, 2001)] assumes instead that the carbon environment provides a set of 1D periodic sites into which the particles settle. Each model's simplification permits direct contact with a body of previous theoreti-

[2]Due to the threefold coordination of the interstitial channel, the potential energy varies with angle ϕ by $\pm 7\%$ at a distance $r=0.2$ Å. The resulting eigenvalue is $\approx 1\%$ lower than is found without taking into account the ϕ dependence (Stan *et al.*, 1998).

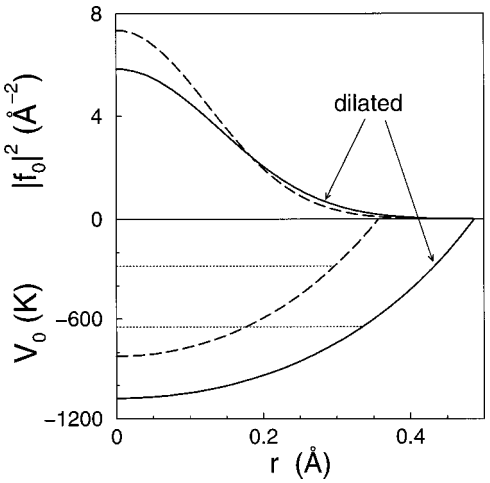

FIG. 4. Angular average of the potential energy (lower panel) and probability density (upper panel) as a function of radial coordinate for H_2 molecules in an interstitial channel corresponding to nanotubes of radius 6.9 Å (dashed curves). Solid curves show results in the case of a 0.5% dilated lattice of nanotubes. The binding energy (horizontal dotted line) is twice as large when the lattice is dilated (Calbi *et al.*, 2000).

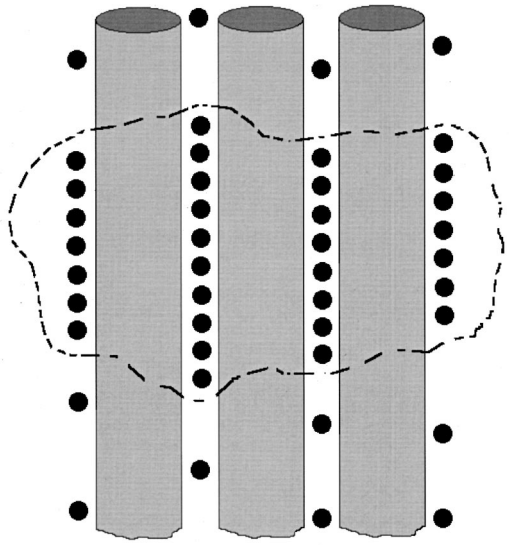

FIG. 5. Schematic depiction of an anisotropic droplet of condensed adsorbate within interstitial channels. The loop represents the boundary of the droplet. This phase results from the interaction between molecules in adjacent interstitial channels.

cal work on 1D models or permits one to solve a new and relatively simple 1D problem (Takahashi, 1999). Particularly interesting is the fact that the localized description represents a realization of the famous lattice gas model in statistical mechanics. In this model, each site may have occupancy zero or one; in the simplest case, only nearest neighbors interact. This model is often applied (perhaps surprisingly) to cases, such as the liquid-vapor transition in free space, for which the model is a significant abstraction of reality. In such cases, the model's limitations are known and attention focuses on the critical regime, for which the essential physics does not suffer from the model's simplifications.

Remarkably, many of the salient features of the collective behavior predicted by the two contradictory models are similar. Both models have the feature that no phase transition occurs at $T \neq 0$ for a system consisting of a single interstitial channel; this is because thermal fluctuations disrupt any hypothetical order in one dimension. At $T=0$, however, transitions for a single interstitial channel may occur as a function of density. For example, within the quasifree 1D model, H_2 undergoes both a condensation and a freezing transition if the free space interaction is assumed (Gordillo *et al.*, 2000); if screening is taken into account (Kostov *et al.*, 2000), however, the condensation transition is suppressed and the single interstitial channel system's ground state is a gas. This remarkable behavior is of great interest, of course, falling into the category of so-called "quantum phase transitions" (Sachdev, 1999).

The interactions between molecules in adjacent interstitial channels is essential to the formation of ordered phases at finite T. Because the separation between interstitial channels is large ($d \approx 10$ Å), this interchannel interaction is quite weak, smaller than the pair well depth by a factor of order $(\sigma/d)^6$, where σ is the molecular diameter. Hence the transverse interaction affects behavior only at low T, but the consequence can be dramatic: phase transitions occur which do not occur without these interactions. Figure 5 depicts such an anisotropic condensed phase that is expected to occur at low T. Carraro has studied the properties of anisotropic crystalline phases arising from the interchannel interaction (Carraro, 2000). Because this interaction is weak, the crystal melts at very low T to a liquid phase, which remains condensed up to a higher temperature. A quantum system (one with weak interactions and light mass, such as He) will not exhibit any such crystalline phase in the absence of an ordering external potential (as is also the case for He in 3D unless pressure is applied), but a liquid phase should occur.

Figure 6 exemplifies the He system's properties, studied within a (localized) anisotropic Ising model. In this model, atoms reside at sites which are closely spaced along the z axis and interact with one another as well as with atoms on adjacent chains (Cole *et al.*, 2000). The interaction perpendicular to the interstitial channels is $\approx 1\%$ of that along the axes. The heat capacity is seen to correspond closely to that of a strictly 1D system (a smooth curve) down to $k_B T/\epsilon \approx 0.25$ ($\epsilon = 10.22$ K for helium). While the strictly 1D system exhibits a gentle maximum in this region, near $k_B T/\epsilon \approx 0.2$, a phase transition occurs in the system with interacting channels. This phase transition is a condensation of the anisotropic fluid, with droplets extending into contiguous channels; indeed they extend a distance equal to the correlation length, which diverges at the critical temperature T_c (see Fig. 6). The value of T_c is high compared to the interchannel interaction temperature ($k_B T_{IC}/\epsilon \approx 0.004$). This follows from the fact that the transition involves a large block of molecules (those within a 1D correlation length) within one interstitial channel inter-

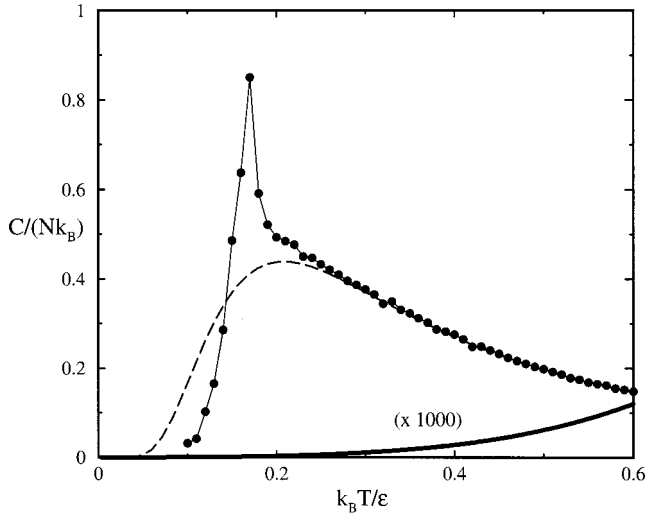

FIG. 6. Specific heat at critical density (solid curve) associated with a condensation of atoms, due to their mutual interactions, within an array of parallel interstitial channels as a function of T relative to the interaction energy along the axis ($\varepsilon \equiv 4J_z$). Monte Carlo calculations (points) suggest a divergence, known to be present in the exact calculation. The dashed curve is the nonsingular specific heat resulting when interactions between atoms in neighboring channels are neglected (i.e., the 1D Ising model). The broad solid curve at the bottom is the lattice specific heat (multiplied by 1000) of a pristine bundle of nanotubes (Cole *et al.*, 2000).

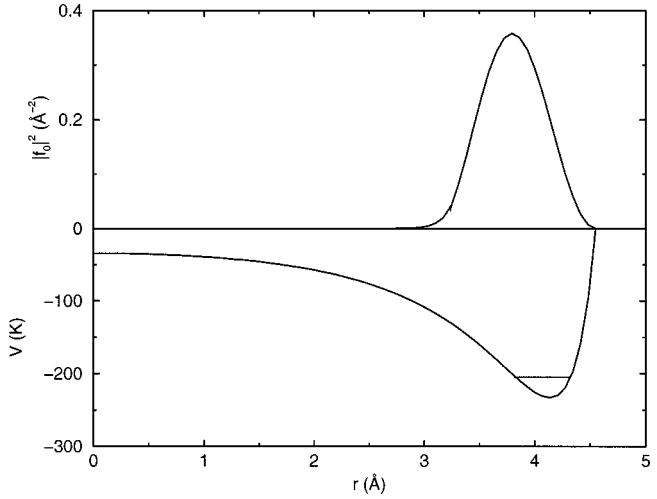

FIG. 7. He ground state in a nanotube. Bottom panel, potential energy and lowest energy level (horizontal line) of a He atom in a nanotube of radius $R=7$ Å; upper panel, the ground-state probability density $|f_0|^2$.

acting with a similar block in an adjacent interstitial channel. An analytic formula derived by Fisher (1967) provides the value of T_c in the limit of strong anisotropy, as is the case here. One of the most interesting features of the transition seen in Fig. 6 is that the heat capacity attributable to the absorbate actually dwarfs that of the host material. The reason is simply that the nanotubes, consisting of strongly cohering carbon, with a Debye temperature ≈ 2000 K, have by themselves only a negligible heat capacity at low T (Mizel *et al.*, 1999).

Figure 4 illustrates another, rather dramatic, effect. Because H_2 molecules are tightly confined within the interstitial channels, their zero point energy of motion perpendicular to the z axis is large. A tiny (0.5%) increase in the spacing between tubes greatly reduces this energy. The net result, including the energy cost of spreading the tubes, is a doubling of the binding energy within the interstitial channels (Calbi *et al.*, 2001). This is a cooperative effect, requiring the presence of many molecules in order to obviate bending of the tubes. The resulting expanded lattice represents the ground state of the system. This expansion of the lattice is perhaps too small to be detected in diffraction (Amelinckx *et al.*, 1999), but it is certainly large enough to be observable in Raman measurements of the tubes' breathing modes (Venkateswaran *et al.*, 1999; Dresselhaus and Eklund, 2000). This sensitivity of the thermodynamic and structural properties to the zero point energy has led Johnson and co-workers to propose using nanotube bundles to separate isotopes of hydrogen (Wang *et al.*, 1999).

III. MATTER WITHIN THE TUBES

A. Cylindrical model

We consider next the behavior of molecules adsorbed within the nanotubes themselves. The presence of such molecules requires that the tubes be open, which occurs if they are prepared appropriately (but not all nanotubes are open, in general). We begin with the single-particle problem of evaluating the potential energy and the corresponding wave functions of the Schrödinger equation. This is a cylindrical surface variant of the familiar "particle in a box" problem. The square of the wave function is the probability density for the particle. As Fig. 7 exemplifies, a molecule with a diameter σ small compared to the tube diameter is bound strongly to the vicinity of the tube wall. This localization in the radial direction justifies a simple "cylindrical model" of the film's properties. Specifically, this model assumes that the particles are confined to the 2D cylindrical surface, $r=R_{eq}$, the equilibrium distance of the particle from the axis.[3] In the classical case, such confinement occurs at low temperature and is described by the Boltzmann factor in the single-particle density distribution ($\sim \exp[-\beta V(r)]$). In the extreme quantum case of He or H_2, the ground state density is spread over a range $\Delta r \approx 0.2$ Å due to the zero-point motion in this potential, as seen in Fig. 7. Even in that case, however, the cylindrical model is useful because the radial degree of freedom is *de facto* frozen out due to the high energy scale associated with radial excitation (≈ 100 K).

Determining the quantum states of the system is easy if we ignore all dependence of the adsorption potential

[3]As exemplified in Fig. 7, the anharmonicity of the potential may give rise to a significant displacement of the position of maximum probability relative to the potential-energy minimum.

on the variables z and φ, the azimuthal angle (Stan and Cole, 1998). With these assumptions, each energy level of a single particle moving on the surface $r=R_{eq}$ is a sum of a constant (the radial ground-state energy E_r), plus azimuthal and axial kinetic energies:

$$E=E_r+E_\varphi+E_z, \tag{5}$$

where

$$E_\varphi=\frac{(\hbar\nu)^2}{2mR_{eq}^2} \tag{6}$$

and

$$E_z=\frac{(\hbar k_z)^2}{2m}. \tag{7}$$

Here, the angular momentum about the z axis is $\nu\hbar$, where ν is zero or an integer. Thus the azimuthal motion is characterized by a discrete spectrum; the gap between the two lowest levels ($\nu=0$ and ±1) corresponds to an azimuthal excitation temperature, $T_\varphi=(\hbar\nu)^2/(2mR_{eq}^2k_B)$, which is of order 1 K for He and H_2 and 0.1 K for Ne. This temperature divides the behavior into a low-temperature regime, for which $\nu=0$, and a high-temperature regime, where a significant range of ν states is populated. For $T\ll T_\varphi$, the only degree of freedom which is excited is that associated with E_z, the quasicontinuous energy of motion parallel to the axis. This regime therefore corresponds to 1D free particle motion. From the analogous problem in 3D, we anticipate the result that the specific heat $c(T)$ (per particle) approaches the 1D limit $c\to k_B/2$ at low temperature. One sees this behavior in Fig. 8; near T_φ the specific heat evolves nonmonotonically[4] from the 1D value to the 2D value, $c=k_B$ (occurring at high T due to excitation of azimuthal motion). This dimensional crossover in the quantum case has no classical analog because it is a consequence of the quantization of azimuthal motion, a wave property.[5,6]

B. Collective properties

Figure 7 hints that particles can reside in either of two regions of space-near the wall or near the axis. We first consider adsorption in a dense "cylindrical shell" phase, localized near the wall. The collective behavior of molecules in this phase is analogous to that within a monolayer film in several respects, but intriguing differences should occur. The specific behavior is sensitive to the species being adsorbed. In some cases, the atomicity of the nanotubes gives rise to a periodic potential ("corrugation") which leads to commensurate phases of the adsorbate, while in other cases, that corrugation can be neglected. This variable behavior is analogous to that on graphite (Bruch *et al.*, 1997), where commensurate phases dominate the monolayer phase diagrams of some adsorbates, like He and H_2, but not others (e.g., Ar). One qualitative difference is that the nanotubes' cylindrical shape yields a periodicity condition that encourages a specific commensurate phase associated with this periodicity (Green and Chamon, 2000).

One of the fundamental questions about the shell phase pertains to the existence and nature of a (finite T) crystalline phase within the tubes comprising a bundle. Recall that a 2D solid is quite different from a 3D solid; the 2D solid is sensitive to long-wavelength fluctuations that prohibit the usual crystalline order. Hence no delta function (Bragg) peaks occur in the x-ray scattering from 2D solids, assuming that no periodic potential is present. Instead, orientational long-range order is permitted in two dimensions, manifested by a quite distinct behavior of the correlation functions, thermodynamic properties, and transverse sound speed. Near melting, for example, the specific heat exhibits an essential singularity rather than the discontinuities characteristic of melting in three dimensions (Strandburg, 1988; Glaser and Clarke, 1993). Since a single nanotube is a 1D system, strictly speaking, we suspect that a hypothetical solid in the tubes is even more sensitive to such fluctuations. The very existence and, certainly, the melting of such a solid are, thus far, unresolved subjects.

For the moment we set aside such questions and focus on manifestations of this geometry which appear to be robust predictions of current theories of this system. One involves the dynamics, i.e., the phonons, of the ad-

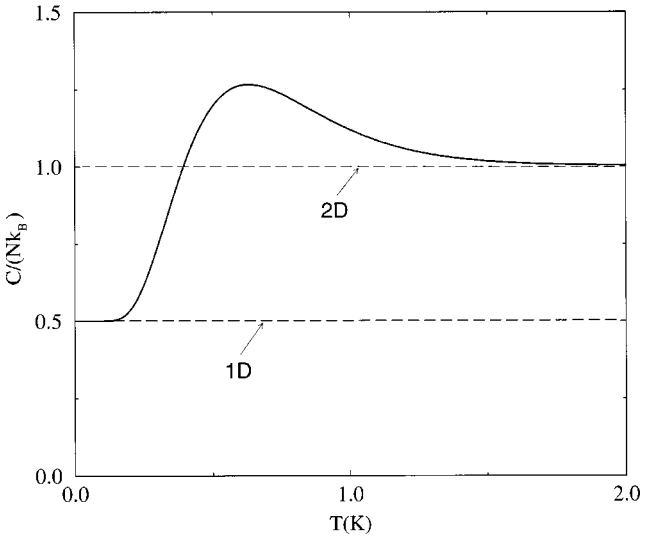

FIG. 8. Specific heat as a function of T of an ultralow-density (see footnote 6) He gas inside a nanotube of radius 5 Å depicting crossover (near $T_\varphi\sim1$ K) from 1D behavior at low T to 2D behavior at high T. From Stan and Cole (1998).

[4]The nonmonotonic behavior in Fig. 8 is similar to that found for $c(T)$ of the linear rotor, for which the eigenvalues vary as $\nu(\nu+1)$, $\nu=0,1,\ldots$. The more familiar monotonic behavior occurs in cases when the energy level spacing is relatively constant.

[5]In contrast, a reduction in dimensionality (from 3D to 2D) associated with particles coalescing onto the cylindrical surface $r=R_{eq}$ occurs for both classical and quantum particles at high temperature.

[6]Note that Fig. 8 shows the classical specific heat, ignoring quantum statistics as well as interactions.

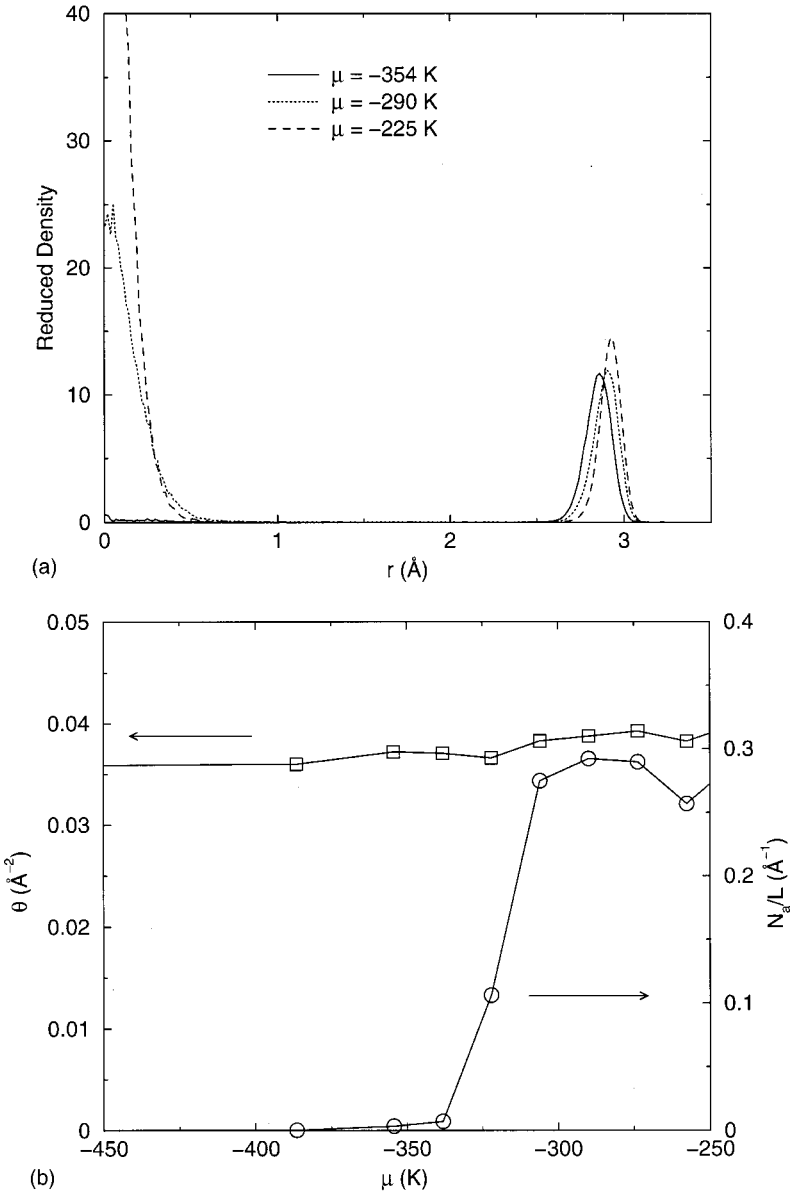

FIG. 9. Density of H_2 molecules at $T=10$ K computed by path-integral Monte Carlo: (a) 3D density as a function of radial distance, inside a nanotube of radius 6 Å for three different values of chemical potential μ. (b) 2D density θ (squares, left scale) of H_2 in shell phase per unit area of tube wall, and 1D density (circles, right scale) of axial phase as a function of chemical potential. From Gatica *et al.* (2000).

sorbate; for specificity, we focus on the long-wavelength and low-energy regime. Each phonon mode possesses an azimuthal quantum number, $\nu=0,\pm1,\pm2,\ldots$, indicating the angular variation of the motion, and a quasicontinuous wave vector (q_z) characterizing its z variation. The lowest energy modes will have no φ variation and thus the excitation spectrum will be 1D in character, associated with the variable q_z. The corresponding low T specific heat will be linear in T (by analogy with the 3D result, which varies as T^3). Vidales *et al.* (1998) have shown how this behavior crosses over to a 2D regime (T^2 dependence) at high T. Not surprisingly, the crossover temperature T_φ can be accurately estimated with a length-matching criterion: at T_φ, the thermal phonon wavelength equals the circumference of the cylindrical surface containing the atoms: $2\pi R_{shell}\approx\hbar c/k_B T$, where c is the speed of sound within the cylindrical shell of radius R_{shell}.

Note that this increase of effective dimension (1D→2D) as T increases is a common feature of the single-particle behavior, discussed earlier, and the phonon behavior. This is not always the case; indeed, the reverse (a decrease of dimensionality) occurs in the previous section's example of a 3D phase transition (because of interactions between particles in adjacent interstitial channels) evolving into 1D behavior at high T (Gelb *et al.*, 1999).

Arguably more unusual than this shell phase is a so-called "axial phase," i.e., molecules confined to the vicinity of the tube's axis (Gatica *et al.*, 2000). The appearance of this phase is exemplified in Figs. 9(a) and 9(b), the results of path integral Monte Carlo calculations of H_2 absorption. The axial phase appears as a rapid increase of density as a function of chemical potential. In some respects, its appearance resembles the layering transition on planar surfaces, but the latter corresponds to a 2D system while the axial phase is 1D. From another point of view, the appearance of the axial phase is closer to the capillary condensation transition exhibited in Fig. 10 (Steele and Bojan, 1998; Gelb *et al.*, 1999).

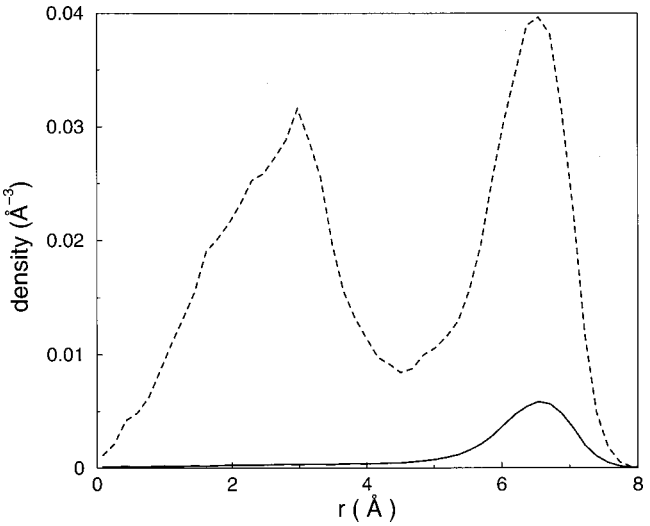

FIG. 10. Density of Kr atoms as a function of distance from the pore axis in a weakly adsorbing cylindrical pore of radius 10 Å. The solid curve is the density distribution at a pressure just below the capillary condensation pressure; the dashed curve corresponds to the filled pore just after condensation (Steele and Bojan, 1998).

While the detailed properties of the axial phase have not been explored, for quantum systems there is the hope that this phase provides a realization of the 1D Luttinger liquid model. That model's novel features include the fact that the low-lying excitation spectrum of even a weakly interacting fermi system (e.g., ^{3}He) is characterized by excitations of Bose type, i.e., phonons (instead of the usual quasiparticles of Fermi-liquid theory). The key qualitative difference between axial phases of ^{3}He and ^{4}He would then be the presence of spin waves in the ^{3}He case.

IV. EXTERNAL SURFACE OF THE NANOTUBE BUNDLE

The external surface of the bundle provides an attractive potential for molecules of all sizes and adsorption will occur there even if the tubes or interstitial channels are closed (Dresselhaus *et al.*, 1999; Gatica *et al.*, 2001). If, instead, they are open, the fraction of particles residing on the external surface depends on the surface to volume ratio, which varies essentially as the inverse of the bundle radius. For a bundle of $\approx$50 tubes, as in Fig. 1, roughly half of the available surface lies on the outer surface. The groove formed by two adjacent tubes at the surface is a particularly favorable environment because the well depth there equals nearly twice that of a single graphene sheet, assuming additivity of the interactions (Talapatra *et al.*, 2000). Figure 11 depicts the potential energy in the case of an Ar atom. One observes a localized deep well, which is the most favored adsorption site in this environment.

Simulation studies have revealed the occurrence of diverse phases on this surface, as seen in Fig. 12. The initial adsorption occurs in the groove, itself; this is a 1D phase, with properties that can be computed from an analytic 1D classical equation of state. At higher pressure, the coverage jumps discontinuously (by a factor of 3) to a so-called "3 stripe" phase, due to the appearance of two new lines of particles parallel to the groove. As the chemical potential increases, a sequence of additional jumps occurs. One represents the formation of a full layer of stripes and the next corresponds to a bilayer's formation. Beyond that point, subsequent growth is qualitatively similar to that of wetting films on the surface of graphite. The transitions seen as vertical risers in Fig. 12 are genuine thermodynamic transitions because the assumed geometry is an infinite plane of perfectly parallel tubes. Surely, there will occur rounding of these discontinuities for any real bundle of tubes. Nevertheless, the real-world phenomena ought to bear a qualitative resemblance to those found in the simulations. The detailed properties of these phases remain to be explored.

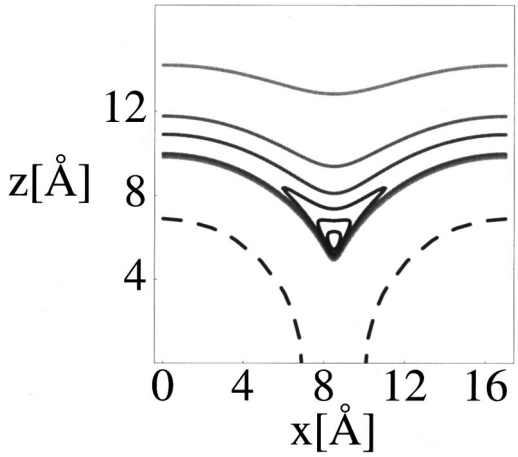

FIG. 11. Groove confinement potential. Solid lines, equipotential energy contours of an Ar atom in the groove, corresponding to constant values $V/\epsilon_{ArC}=-25, -20, -15, -10, -5, -1$, from darker to lighter, where $\epsilon_{ArC}=58$ K; dashed lines, cylindrical nanotube surfaces containing the carbon atoms.

V. SUMMARY

In this Colloquium we have chosen a few phenomena to illustrate the rich physics present in this unusual ge-

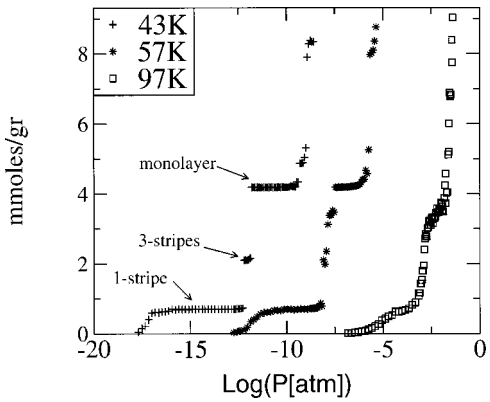

FIG. 12. Phase transitions occurring within Kr atoms adsorbed on the external surface of the nanotube bundle, manifested as discontinuities in coverage (expressed in adsorbate mmoles per gram of carbon) as a function of pressure. The stable values of coverage correspond to striped phases, lying parallel to the grooves between external tubes. From Gatica *et al.* (2001).

ometry. Every aspect of the problem has stimulated its own branch of the theory "tree": our selection of topics reflects our bias. We encourage newcomers to this field to find their own branch and explore territory as fertile as that discussed here.

The exotic scenarios described in this Colloquium are based on a sequence of simplifying approximations, each of which merits scrutiny. For example, the adsorption potentials have been derived by simply summing empirical interactions between the adatoms and the individual carbons comprising the tubes. Although significant quantitative uncertainty results from this neglect of many-body effects (Kostov *et al.*, 2000), we are optimistically inclined to regard many of the qualitative predictions as robust. A more serious concern, in our opinion, is the assumption that the nanotubes are chemically and structurally perfect, forming a periodic array. This is not at all the case for currently available samples. We believe that the possibility of observing the zoo of phase transition phenomena discussed here is a strong motivation for improving sample quality. On the other hand, the effects of disorder on phase transitions is a very important subject. Hence experimentalists are urged to explore the phenomena as a function of sample preparation; we are confident that theorists will be delighted to see their data.

ACKNOWLEDGMENTS

Our work has been stimulated by discussions with many colleagues and workers in this field. We are particularly grateful to Jayanth Banavar, Jordi Boronat, Michel Bienfait, Massimo Boninsegni, Carlo Carraro, Moses Chan, Vin Crespi, Peter Eklund, Carmen Gordillo, Bob Hallock, Karl Johnson, Susana Hernandez, Milen Kostov, Aldo Migone, Ari Mizel, Dave Narehood, Paul Sokol, Bill Steele, Flavio Toigo, and Keith Williams. This research has been supported by the Army Research Office, Fundación Antorchas, CONICET, the National Science Foundation, and the Petroleum Research Fund of the American Chemical Society.

REFERENCES

Amelinckx, S., A. A. Lucas, and P. Lambin, 1999, Rep. Prog. Phys. **62**, 1471.

Bienfait, M., B. Asmussen, M. Johnson, and P. Zeppenfeld, 2000, Surf. Sci. **460**, 243.

Boninsegni, M., S.-Y. Lee, and V. H. Crespi, 2001, Phys. Rev. Lett. **86**, 3360.

Bruch, L. W., M. W. Cole, and E. Zaremba, 1997, *Physical Adsorption: Forces and Phenomena*, Intl. Series Monographs in Chemistry No. 33 (Oxford University Press, Oxford).

Calbi, M. M., Flavio Toigo, and Milton W. Cole, 2001, Phys. Rev. Lett. **86**, 5062.

Carraro, C., 2000, Phys. Rev. B **61**, R16 351.

Cole, M. W., V. H. Crespi, G. Stan, J. M. Hartman, S. Moroni, and M. Boninsegni, 2000, Phys. Rev. Lett. **84**, 3887.

Dillon, A. C., and M. J. Heben, 2001, Appl. Phys. A: Mater. Sci. Process. **72**, 133.

Dresselhaus, M. S., G. Dresselhaus, and P. C. Eklund, 1996, *The Science of Fullerenes and Carbon Nanotubes* (Academic Press, New York).

Dresselhaus, M. S., and P. C. Eklund, 2000, Adv. Phys. **49**, 705.

Dresselhaus, M. S., K. A. Williams, and P. C. Eklund, 1999, MRS Bull. **24**, 45.

Fisher, M. E., 1967, Phys. Rev. **162**, 480.

Gatica, S. M., M. J. Bojan, G. Stan, and M. W. Cole, 2001, J. Chem. Phys. **114**, 3765.

Gatica, S. M., G. Stan, M. M. Calbi, J. K. Johnson, and M. W. Cole, 2000, J. Low Temp. Phys. **120**, 337.

Gelb, L. D., K. E. Gubbins, R. Radhakrishnan, and M. Sliwinska-Bartkowiak, 1999, Rep. Prog. Phys. **62**, 1573.

Glaser, M. L., and N. A. Clarke, 1993, Adv. Chem. Phys. **83**, 543.

Gordillo, M. C., J. Boronat, and J. Casulleras, 2000, Phys. Rev. Lett. **85**, 2348.

Green, D., and C. Chamon, 2000, Phys. Rev. Lett. **85**, 4128.

Iijima, S., 1991, Nature (London) **354**, 56.

Kostov, M. K., M. W. Cole, J. C. Lewis, P. Diep, and J. K. Johnson, 2000, Chem. Phys. Lett. **332**, 26.

Kuznetsova, A., J. T. Yates, Jr., J. Liu, and R. E. Smalley, 2000, J. Chem. Phys. **112**, 9590.

Mizel, A., L. X. Benedict, M. L. Cohen, S. Louie, A. Zettl, N. K. Budraa, and W. P. Beyermann, 1999, Phys. Rev. B **60**, 3264.

Muris, M., N. Dufau, M. Bienfait, N. Dupont-Pavlovsky, Y. Grillet, and J. P. Palmari, 2000, Langmuir **16**, 7019.

Sachdev, S., 1999, *Quantum Phase Transitions* (Cambridge University Press, Cambridge, England).

Schlittler, R. R., J. W. Seo, J. K. Gimzewski, C. Durkan, M. S. M. Saifullah, and M. E. Welland, 2001, Science **292**, 1136.

Stan, G., M. J. Bojan, S. Curtarolo, S. M. Gatica, and M. W. Cole, 2000, Phys. Rev. B **62**, 2173.

Stan, G., and M. W. Cole, 1998, Surf. Sci. **395**, 280.

Stan, G., V. H. Crespi, M. W. Cole, and M. Boninsegni, 1998, J. Low Temp. Phys. **113**, 447.

Steele, W. A., and M. J. Bojan, 1998, Adv. Colloid Interface Sci. **76-77**, 153.

Strandburg, K. J., 1988, Rev. Mod. Phys. **60**, 161.

Takahashi, M., 1999, *Thermodynamics of 1D Solvable Models* (Cambridge University Press, Cambridge, England).

Talapatra, S., A. Zambano, S. E. Weber, and A. D. Migone, 2000, Phys. Rev. Lett. **85**, 138.

Teizer, W., R. B. Hallock, E. Dujardin, and T. W. Ebbesen, 1999, Phys. Rev. Lett. **82**, 5305.

Teizer, W., R. B. Hallock, E. Dujardin, and T. W. Ebbesen, 2000, Phys. Rev. Lett. **84**, 1844.

Venkateswaran, U. D., A. M. Rao, E. Richter, M. Menon, A. Rinzler, R. E. Smalley, and P. C. Eklund, 1999, Phys. Rev. B **59**, 10 928.

Vidales, A. M., V. H. Crespi, and M. W. Cole, 1998, Phys. Rev. B **58**, 13 426.

Wang, Q., S. R. Challa, D. S. Sholl, and J. K. Johnson, 1999, Phys. Rev. Lett. **82**, 956.

Weber, S. E., S. Talapatra, C. Journet, A. Z. Zambano, and A. D. Migone, 2000, Phys. Rev. B **61**, 13 150.

Williams, K. A., and P. C. Eklund, 2000, Chem. Phys. Lett. **320**, 352.